ELECTRICAL ENGINEERING DEPARTMENT

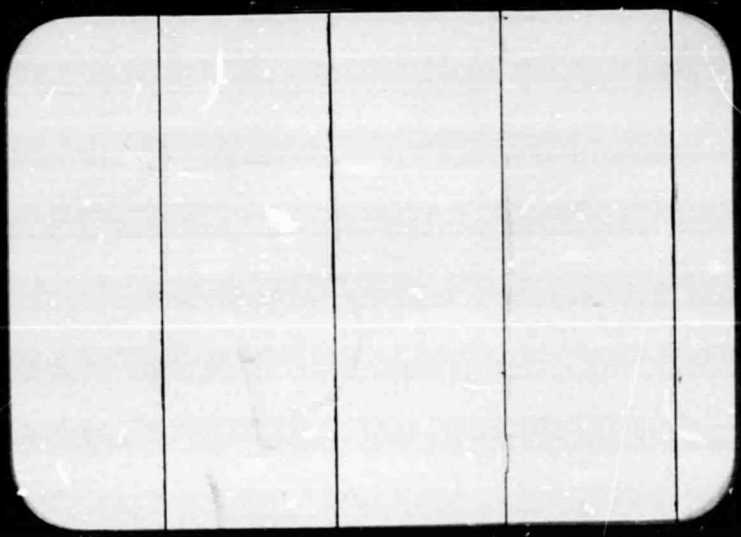

UNIVERSITY OF TENNESSEE

KNOXVILLE TN 37916

Prepared For

George C. Marshall Space Flight Center
National Aeronautics and Space Administration
Under Contract NAS8-27296/DCN 1-1-40-10230

DEVELOPMENT OF A DIGITAL ELECTRONIC REBALANCE LOOP FOR A DRY TUNED-ROTOR TWO DEGREE-OF-FREEDOM GYROSCOPE

T. V. Blalock, E. J. Kennedy
V. A. Thomason

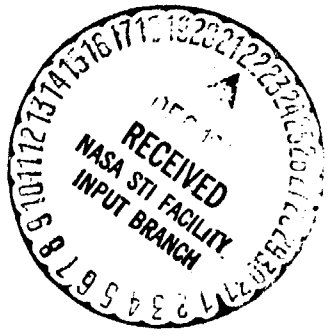

Technical Report TR-EE/EL-5
September 29, 1975

ACKNOWLEDGEMENTS

The authors are very appreciative of the assistance provided by many of the staff of the Astrionics Laboratory, Marshall Space Flight Center, NASA. The advice and guidance of the Co-ordinator, Mr. E. H. Berry, was especially significant. We also wish to acknowledge the design improvements to the Digital Control Electronics (DCE) system provided by Mr. Harry Reed, and particularly the excellent design for the DC-to-DC Converter power supply furnished by Mr. Bill Baker, both of MSFC.

The authors thank Mrs. Debbie Lenarduzzi for her skillful typing of this report.

DEVELOPMENT OF A
DIGITAL ELECTRONIC REBALANCE LOOP
FOR A DRY TUNED-ROTOR
TWO DEGREE-OF-FREEDOM GYROSCOPE

ABSTRACT

Digital electronic rebalance loops were designed and implemented in brassboard form to capture both X and Y axes of the Kearfott Gyroflex. The loops were width-modulated binary types using a 614.4 kHz keying signal and a 2.4 kHz sample frequency. The loops were designed for a torquing rate of 2°/sec (70.6 mA torquing current) and a data resolution of 23.4 milli-arc-sec per data pulse. Design considerations, implementation details, and preliminary experimental results are presented.

TABLE OF CONTENTS

LIST OF FIGURES

LIST OF SYMBOLS

Symbol	Description	Units
ΔA_q	Increment in torque current area	mA-sec/data pulse
B	Elastic restraining torque	dyne-cm/rad
ENV_{sd}	Equivalent noise voltage at synchronous demod. input	volt/$Hz^{1/2}$
ENV_p	Equivalent noise voltage of preamplifier	volt/$Hz^{1/2}$
e_{nc}	Noise voltage at ESP output	volts rms
F	Damping coefficient	dyne-cm-sec/rad
f_i	Interrogation frequency	Hz
f_{cl}	Closed-loop bandwidth	Hz
f_{sg}	Pickoff frequency	Hz
f_z	Frequency of s-domain zero	Hz
f_p	Frequency of s-domain pole	Hz
Δf_{bn}	Noise bandwidth of the bandpass filter	Hz
Δf_n	Noise bandwidth of the G_{dc} block	Hz
G_{dc}	DC amplifier and compensator transfer function	volts dc/volt dc
G_p	Preamplifier gain	volts rms/volt rms
G_b	Bandpass filter gain	volts rms/volt rms
G_a	AC amplifier gain	volts rms/volt rms
G_{sd}	Synchronous demodulator gain	volts dc/volt rms
G_{ct}	Pulse width modulator transfer function	mA/volt dc
G_{pc}	Error signal processor transfer function	volts dc/volt rms

Symbol	Description	Units
G_l	Loop transmission	volts/volt
G_{ac}	Gain of ac section of ESP	volts rms/volt rms
G_m	Gain margin	dB
Δg	Accelerometer data resolution	g/data pulse
H_g	Inertial mass transfer function	rad/dyne-cm
H_{tgp}	Inertial sensor transfer function	rms volts/mA
I	Torque current level	mA
J	Mass moment of inertia	dyne-cm-sec^2/rad
k_p	Pickoff scale factor	rms volts/rad
k_t	Torquer scale factor	dyne-cm/mA
k_t'	Torquer scale factor	deg/mA-sec
k_{dc}	DC amplifier and compensator gain constant	volts dc/volt dc
k_{pc}	Error signal processor gain constant	volts dc/volt rms
k_{oi}	Gyro gain	rad/rad
k_a	Accelerometer scale factor	mA/g
R	Ramp slope	volts/sec
R_d	Data rate	pulses/sec
s	Laplace transform variable	rad/sec
T	Torque	dyne-cm
t_i	Interrogation period	sec
ΔT_A	Increment in torque area	dyne-cm-sec
ΔV_{cq}	Data quantization	volts/data pulse
ΔV_{ptcr}	Torque current ripple at pickoff output	volts peak

Symbol	Description	Units
ΔV_{tcr}	Torque current ripple at pickoff output	volts rms
ΔV_{tcro}	Torque current ripple at ESP output	volts rms
V_{sg}	Pickoff excitation	volts rms
V_c	Error signal processor output voltage	volts dc
ϵ_n	Random noise inaccuracy	rms data pulses
ϵ_{dc}	DC offset inaccuracy	data pulses
θ	Angle	rad
$\Delta\theta_d$	Gyro data resolution	arc-sec/data pulse
$\Delta\theta_{di}$	Gyro input axis resolution	arc-sec/data pulse
θ_m	Phase margin	degrees
τ_t	Torquer time constant	sec
τ_z	Time constant of s domain zero	sec
τ_p	Time constant of s domain pole	sec

CHAPTER I

INTRODUCTION

The design theory and experiences presented in our 1973-74 contract report (1) were used in the development of a new digital electronic rebalance loop for a dry tuned-rotor two degree-of-freedom gyroscope the Kearfott Gyroflex, S/N 4993. A complete system consisting of a rebalance loop for each axis was implemented in brassboard form and delivered to MSFC September 9, 1975.

The new rebalance loop maintains the versatility of previous designs so that loop parameters can easily be adjusted to vary operating conditions for a single gyro or accomodate a range of different gyros. The loops were also designed for microcircuit implementation.

The basic organization of our rebalance loops is shown in Fig. 1. The two Gyroflex loops (X and Y) share one digital control logic section but have separate error signal processors and pulse width modulators as shown in Fig. 2. The basic elements of each loop are the same as those published previously (1), and are shown in Fig. 3.

Very little design theory is presented in this report since it has been published previously in our 1973-74 report (1). In this report we present the design considerations for the Gyroflex loop, the implementation details of each part of the loop, the evaluation of the performance of the breadboard implementation of the loop, and some conclusions and recommendations. We consider our experimental results preliminary until more quantitative results are obtained at MSFC with precision rate tables.

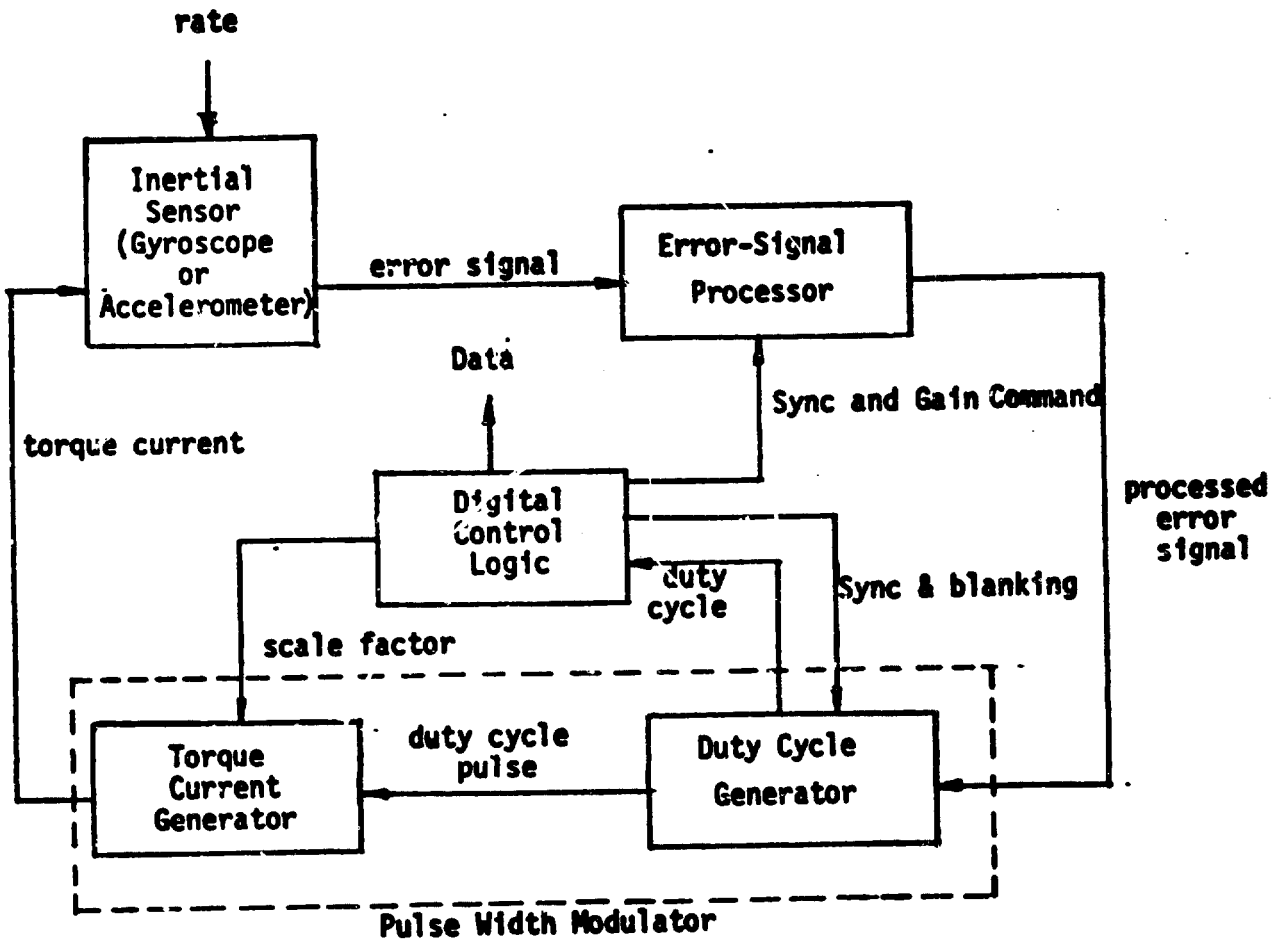

Figure 1. Basic Organization of a Width-Modulated Binary Pulse Rebalance Electronics Loop.

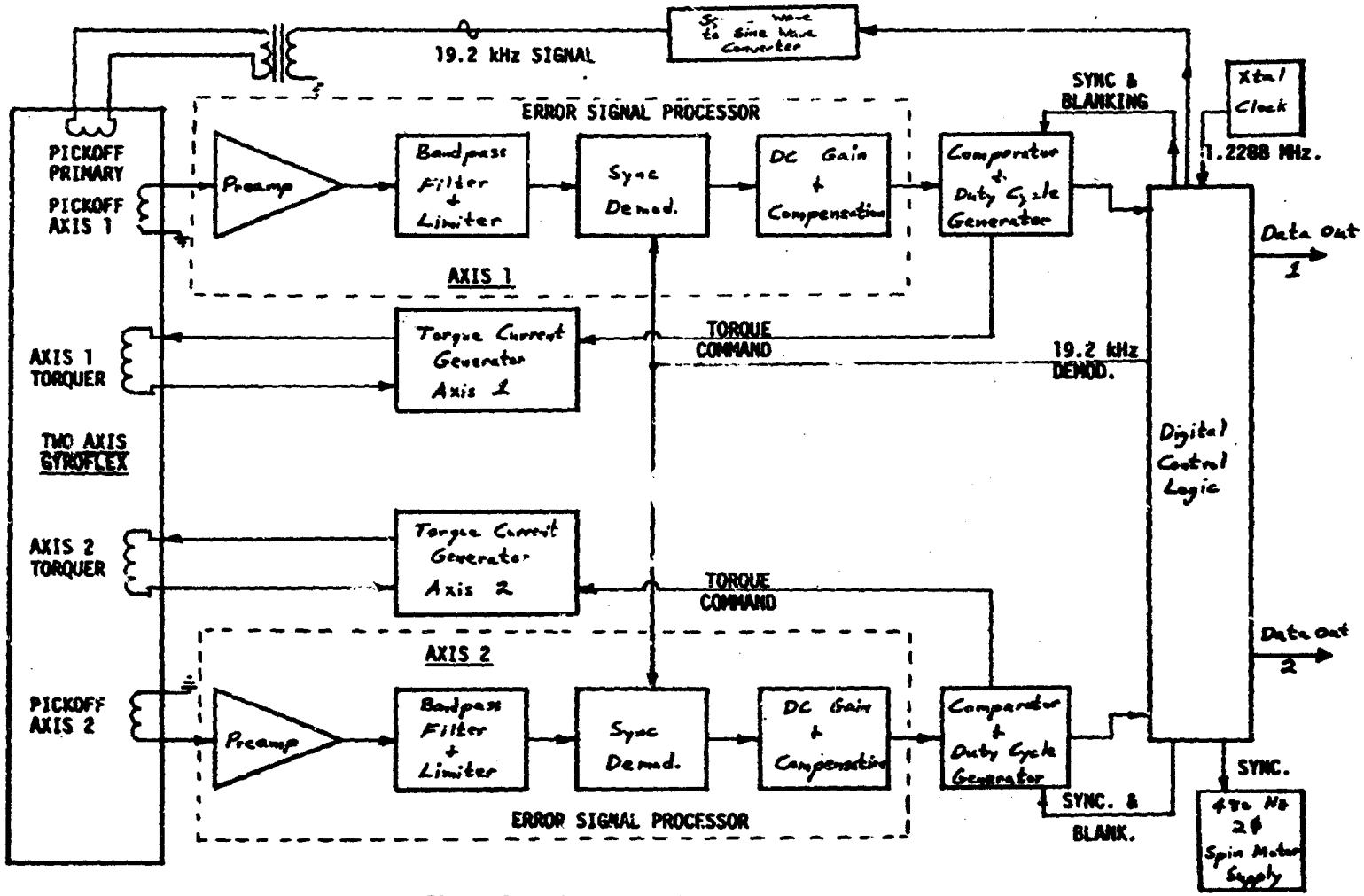

Figure 2. UTK Width-Modulated-Binary Pulse Rebalance System for the Gyroflex.

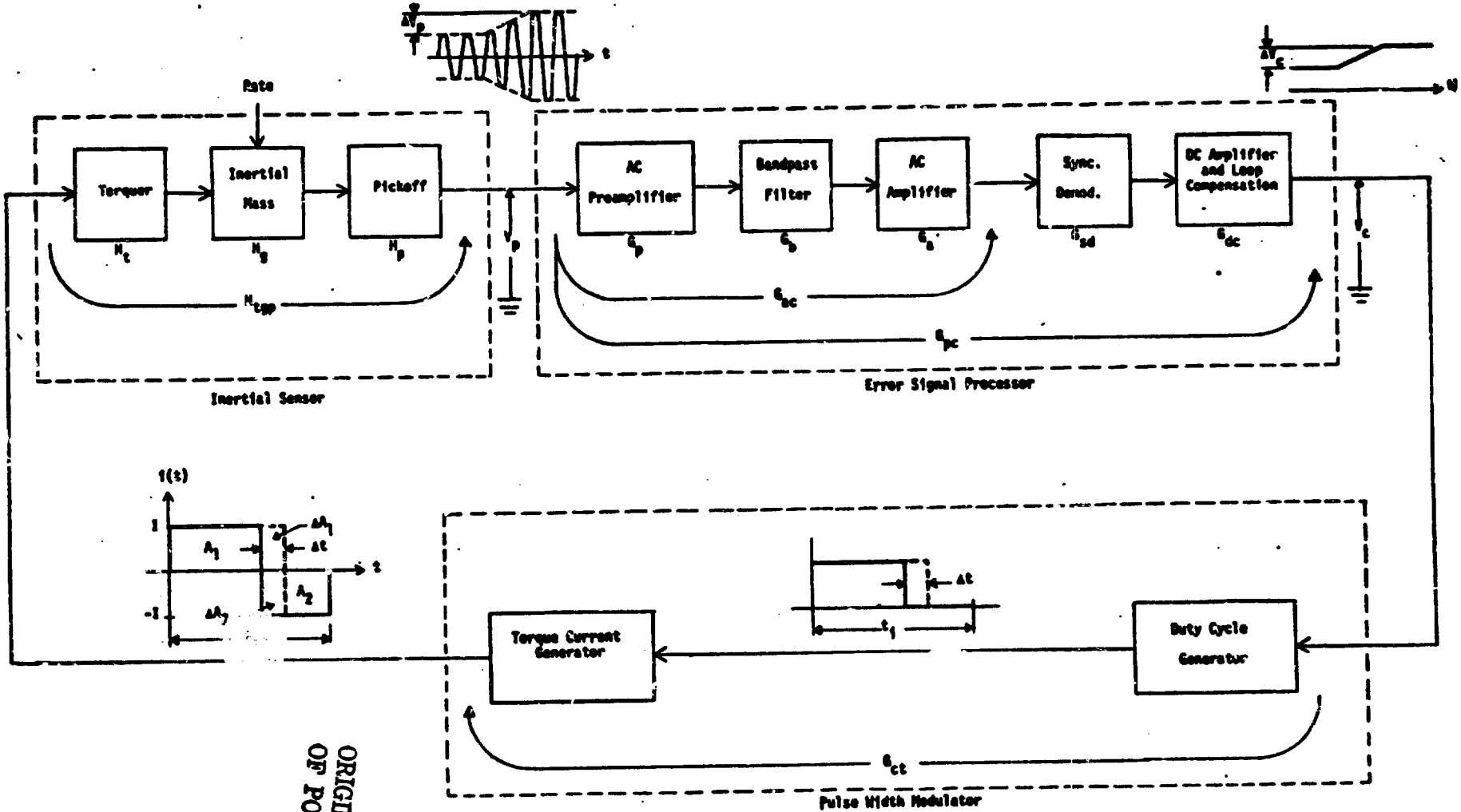

Figure 3. The Basic Elements of the UTK Width-Modulated Binary Rebalance Loops.

CHAPTER II

DESIGN OF A REBALANCE LOOP FOR THE KEARFOTT GYROFLEX

The information available on the parameters of the Gyroflex model was too sparse to allow a detailed design of cross-coupled rebalance loops. Thus, we decided to design an easily adjustable single rebalance loop assuming no interaction between axes within the inertial sensor. This loop could then be used to investigate the dynamic response of the gyro under closed-loop conditions and to specifically evaluate the degree of interaction.

Using the values of gyro parameters in Table I, yields the transfer function from torquer input to pickoff output for the y axis:

$$H_{tgp}(f) = \frac{2.98 \times 10^{-3}}{jf(1+j\frac{f}{0.031})(1+j\frac{f}{7960})} \quad \text{(rms volts/mA)}. \qquad (1)$$

The second gyro corner frequency of f_g=0.031Hz required a simple zero and several poles in the first Error Signal Processor (ESP) design. Closed loop measurements with the first ESP used with the Gyroflex indicated that f_g was greater than 10Hz but that the scale factor (2.98×10^{-3}) of Eq. (1) was nearly correct (measured value $\approx 2.5 \times 10^{-3}$). This higher value of f_g allowed the elimination of the zero in the first ESP compensator.

The Bode diagram of the loop transmission synthesized for the breadboard implementation is shown in Fig. 4. The ESP was designed for a system closed-loop response of 5Hz, phase margin of 75° and gain margin of 14db. An integrator with integration zero at f = 0.55Hz was included in

TABLE I

INERTIAL SENSOR PARAMETERS - GYROFLEX

Parameter	S/N 4993		S/N 4145	
	X Axis	Y Axis	X Axis	Y Axis
J - mass moment of inertia dyne-cm-sec^2/rad			$2.76 \times 10^{4*}$	$4.16 \times 10^{4*}$
F - damping coefficient dyne-cm-sec/rad			$0.8 \times 10^{4*}$	$0.8 \times 10^{4*}$
B - elastic restraining torque dyne-cm/rad	negligible	negligible		
K'_p - pickoff sensitivity rms volts/deg	.66	.66		
τ_t - torquer time-constant msec	0.020	0.020		
K'_t - torquer scale factor deg./mA-sec	0.0283	0.0283		
R - Main Torquer Resistance-25°C ohms	314.	299.		
R - Main Torquer Resistance-65°C ohms	364.	347.		
f_{sg} - pickoff frequency kHz	19.2	19.2		
V_{sg} - pickoff excitation rms volts	2.5	2.5		
P.O. Output Resistance - 65°C ohms	153.	153.		
Main Torquer Inductance - 65°C mH at 20 kHz	7.3	7.2		
P.O. Input Resistance - 65°C ohms at 19.2 kHz	27.4	27.4		
Spin Motor Frequency - Hz	480.	480.		

*Data from R.F. Cimera, Trip Report, Ref. 2.

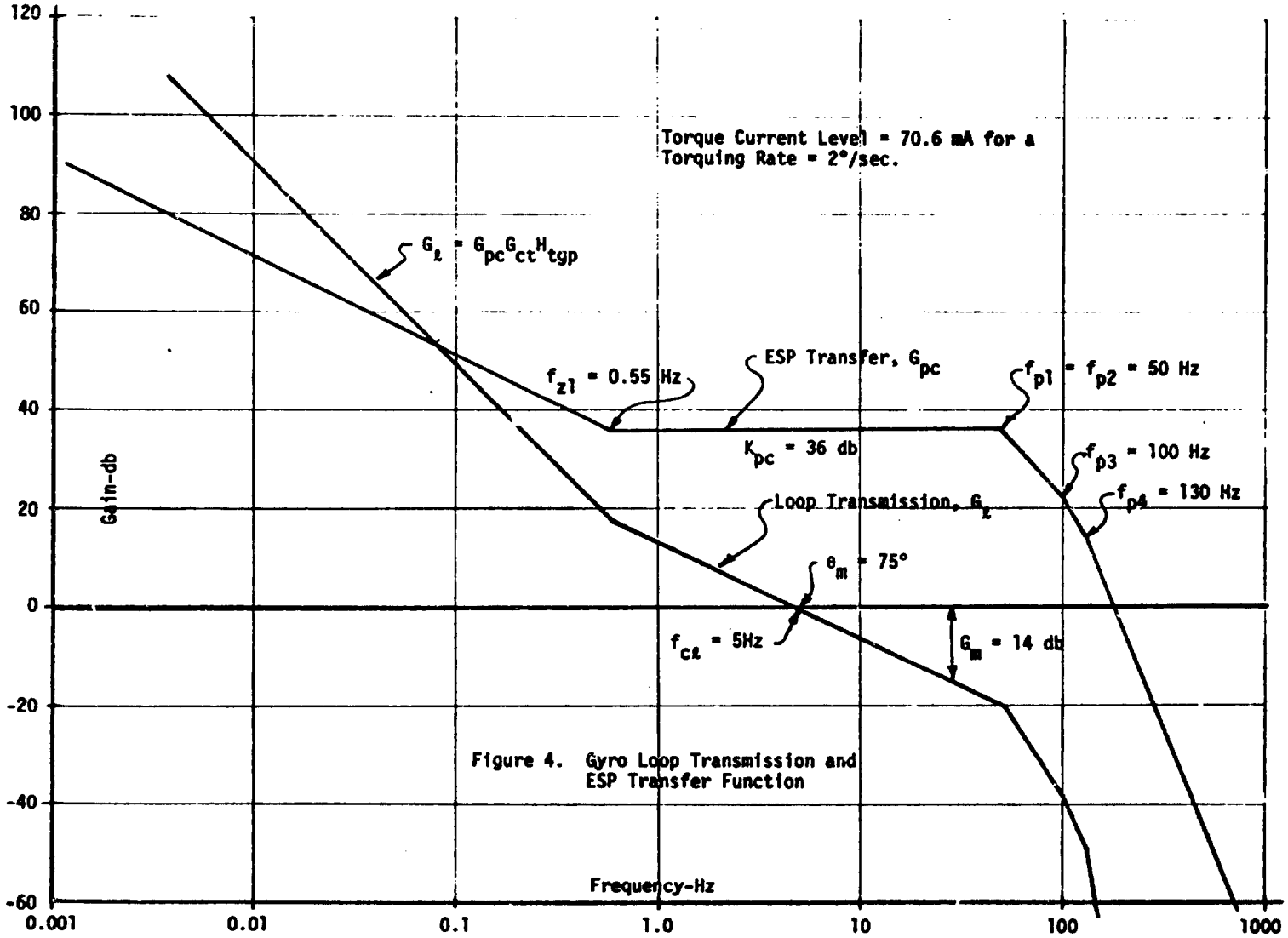

Figure 4. Gyro Loop Transmission and ESP Transfer Function

the ESP transfer to provide a very high loop gain at low frequencies (≈ 90db at 0.01 Hz). A cluster of four poles between 50 and 130Hz were synthesized to discriminate against N, 2N, etc. spin frequencies (N = 240Hz for the gyro spin motor powered by a 480Hz two-phase supply) and to also limit the bandwidth presented to pickup and random noise. The transfer function of the ESP was designed to be

$$G_{pc} = \frac{63(1+j\frac{f}{0.55})}{(\frac{jf}{.55})(1+j\frac{f}{50})^2(1+j\frac{f}{100})(1+j\frac{f}{130})} \quad (\frac{\text{Volts dc}}{\text{Volts rms}}). \qquad (2)$$

Basic system parameters were kept the same as in previously developed systems (1): the data rate R_d is 614.4 kpps, interrogation frequency f_i = 2.4kHz, ramp slope R = 10^4 V/sec, and data quantization ΔV_{cq} = 16.3 mV/data pulse.

The torquing rate was set at 2°/sec to limit the required voltage supply to the H-switch to 40 volts to protect the H-switch transistors from possible voltage breakdown. A major disadvantage of the gyro used for this feasibility study was its high torquer resistance which of course necessitates the use of high H-switch voltages.

The torque current level of 70.6 mA required for a torquing rate of 2°/sec caused the data resolution θ_d to be (1)

$$\theta_d = \frac{7200I}{R_d} K_t' = 23.4 \text{ milli-arc-sec.} \qquad (3)$$

The torque current ripple V_{tcro} at the output of the ESP is given by (1)

$$\Delta V_{tcro} = \frac{K_t' K_p' I}{4\sqrt{2}\, f_i} \, |Gpc(f_i)|. \qquad (4)$$

The value of $|Gpc(f_i)|$ is calculated from Eq. (2) and is approximately 6.17×10^{-5}. Then

$$\Delta V_{tcro} \approx 6 \times 10^{-9} \text{ volts},$$

which is negligibly small.

The uncertainty due to electronic noise is usually caused primarily by noise generated in the preamplifier circuit; however, the integrator in the output section of the ESP (Fig. 5) can cause an emphasis on the low frequency noise produced in the directly coupled section of the ESP. First consider the preamplifier contribution computed with the help of (1)

$$e_{ncp} = \sqrt{(ENV_p)^2 (K_{pc})^2 \Delta f_n}. \qquad (5)$$

The ENV_p of the preamp is due to the IC1A (Fig. 5) RC4136 with white noise ENV $\approx$ 10 nV/Hz$^{1/2}$ and the resistor R_1 = 3K. The total ENV_p is therefore about 12.3 nV/Hz$^{1/2}$. From Fig. 4, the noise bandwidth Δf_n is about 50Hz and K_{pc} = 63. Thus,

$$e_{ncp} \approx 5.5 \ \mu V \ \text{ rms},$$

which is equivalent to 3.37×10^{-4} rms data pulse.

Low-frequency noise generated in the directly coupled section of the ESP ($G_{sd}\ G_{dc}$) would be strongly amplified by the integrator in the G_{dc} block if high gain did not precede the d-c block. The gain preceeding the $G_{sd}\ G_{dc}$ block is $Av_1 = G_{ct}\ H_{tgp}\ G_{ac}$ which in our design is

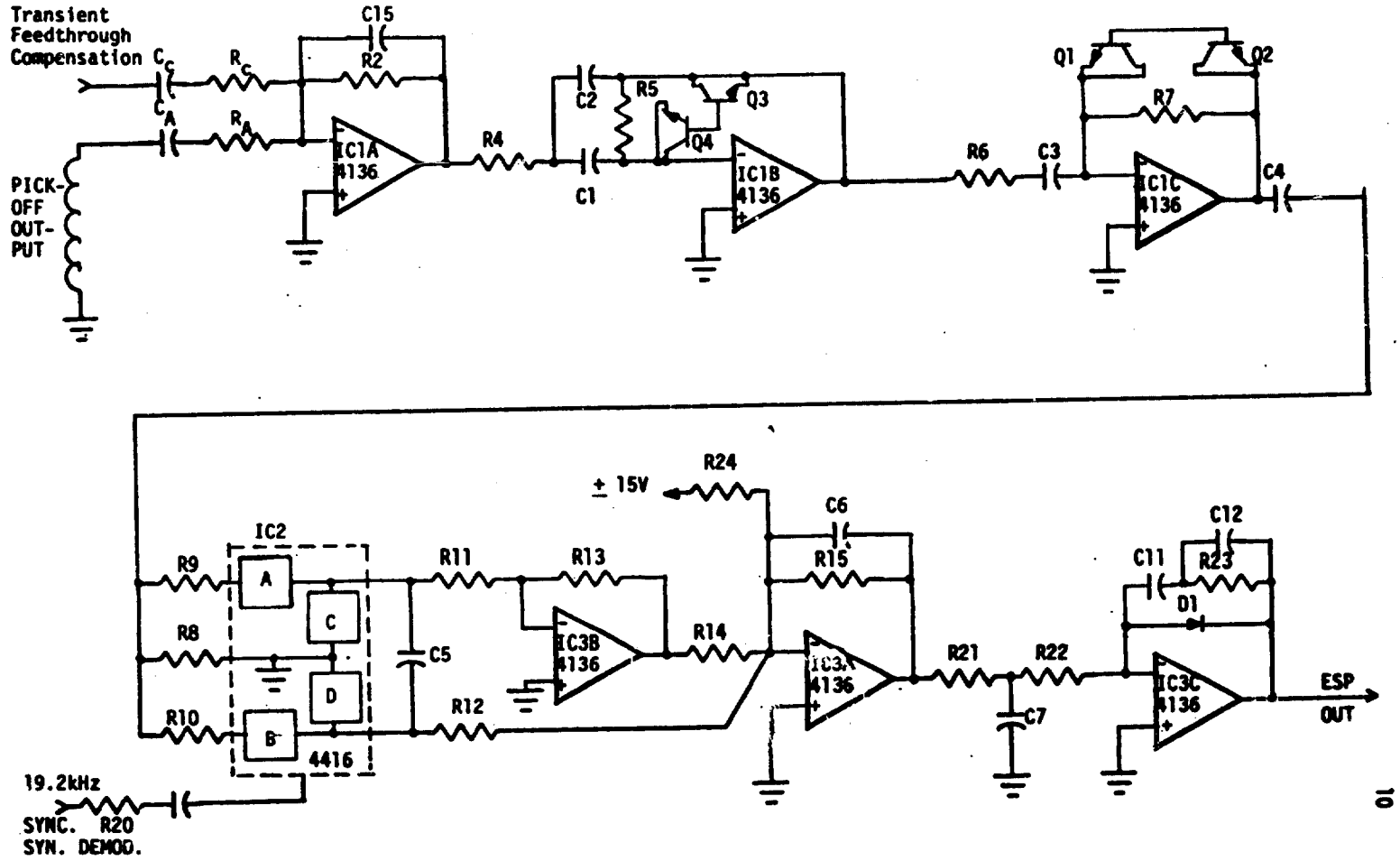

Figure 5. Error Signal Processor-Gyroflex

$$(35)\ \left(\frac{2.5 \times 10^{-3}}{jf}\right)(45) = \frac{3.9}{jf} \qquad (6)$$

at low frequencies. The RC4136 Op Amps have a low-frequency noise component that becomes significant below 10Hz and is specified to be 1000 $nV/Hz^{1/2}$ at 1Hz. There are three RC4136 Op Amps in the output dc section (Fig. 5) so that the ENV at 1Hz at the input to the d-c block is approximately 1732 $nV/Hz^{1/2}$. At the ESP output the noise spectral density would be flat at about 456 $nV/Hz^{1/2}$ if the low-frequency spectrum is assumed to be the typical spectrum expressed by

$$ENV_{\text{low freq.}} = \frac{K}{f}\ , \qquad (7)$$

between f = 1Hz and f = 10Hz. Therefore, the low-frequency noise component at the ESP output in the 10Hz bandwidth will be about

$$e_{n\ell f} = (456)\sqrt{10} = 1.44\ \mu V\ \text{rms}, \qquad (8)$$

which is equivalent to 0.89×10^{-4} rms data pulse. The total expected uncertainty caused by random electronic noise generated in the ESP is a quadratic sum of the Eq. (5) and Eq. (8) values or

$$e_n = 3.54 \times 10^{-4}\ \text{rms data pulse.}$$

The uncertainty due to dc offsets can be computed from (1)

$$\varepsilon_{dc} = \frac{\Delta V_{dcsd}}{\Delta V_{cq}\ H_{tgp}(0)\ G_{ct}\ G_{ac}} \qquad (9)$$

when ΔV_{dcsd} is the total offset voltage of the $G_{sd}\ G_{dc}$ block referred to the input to the synchronous demodulator. Taking the worse-case value of bias current of 500 nA and offset voltage of 0.6 mV for the RC4136 Op Amps (Fig. 5)

gives $V_{dcsd_{max}} \approx 157$ mV. The value of $H_{tgp}(0)$ is unknown since a value of the spring constant B is unknown; therefore, take $H_{tgp}(0) = H_{tgp}(0.001Hz)$. Then using Eq. 6,

$$e_{dc_{max}} = 2.5 \times 10^{-3} \text{ data pulse.}$$

This is a significant static error of 2500ppm and must be compensated by the offset balance circuit (R24) in the ESP (Fig. 5).

CHAPTER III

IMPLEMENTATION OF THE REBALANCE LOOPS

The basic configuration of the various sections of each of the rebalance loops are very similar to those published and discussed in detail in Reference (1). Therefore, the discussions presented here will emphasize significant differences between these loops (new design) and those published previously (old design).

Error Signal Processor (ESP)

As shown in Fig. 5, the ESP is composed of a preamplifier (IC1A), bandpass filter (IC1B), ac amplifier (IC1C), and the combination synchronous demodulator-loop compensator (IC2, IC3B, IC3A, IC3C).

The preamplifier is a new design which uses one section of the RC 4136 quad op-amp connected in an inverting, single-ended input with provision for both quadrature and transient feed-through compensation with the RC networks R_Q, C_Q and R_c, C_c (Fig. 5). A differential input is not needed since the pickoff output has one side grounded. The low value of ESP midband gain removes the low-noise requirement for the preamplifier so that ordinary op-amps could be used in a relatively unsophisticated feedback configuration.

The bandpass filter and ac amplifier are old designs which incorporate the overload clamps (Q_1, Q_2, Q_3, Q_4) to give minimum phase shift of the signal under all overload conditions. Design adjustments of midband gain were accomplished by properly choosing the values of R_6 and R_7 in the ac amplifier.

The synchronous demodulator uses inexpensive op-amps IC3B and IC3A in a differential configuration with part of the loop compensation included in

the configuration. This new design has one pole at 130 Hz set by C5 connected directly across the output of the IC2 switch. This technique relaxes the dynamic range requirements of the differential amplifier. Capacitor C6 in the output op-amp of the differential configuration establishes another pole at 100 Hz. Capacitors C7 and C12 each establish a pole at 50 Hz. The op-amp circuit associated with IC3C also has a zero at 0.55 Hz to provide low-frequency integration with a consequent very high low-frequency gain that produces small hang-off of the gyro rotor.

All the ESP functions are realized with only three IC blocks: one SCL4416 CMOS switch, and two RC4136 quad op-amp blocks. Therefore, there are two spare RC4136 op-amps that could be used to realize a more complex compensator pole-zero constellation or perhaps active notch filters that may be needed to suppress spin motor frequencies in some gyros. Tht ESP design is quite versatile; consequently, a wide variety of transfer functions can easily be implemented with minor circuit changes.

Torque Current Generator (TCG)

The TCG provides a precision current to the torquer winding of the gyro, with a time duration controlled by the input torque command signal from the Digital Control Electronics (DCE) board.

The schematic diagram for the TCG for the Kearfott Gyroflex is shown in Figure 6. This circuit is quite different from that used in the basic design of last years work (1), primarily because of the much higher power supply voltage (40V instead of the earlier 15 V) required for the current source transistor Q14. For a nominal full-scale torque requirement of 2°/sec, the torque current is 70.6 mA. For the Gyroflex unit the torquer resistance is typically 377-ohms (we measured actually 363.7 and 346.7 for the X and Y

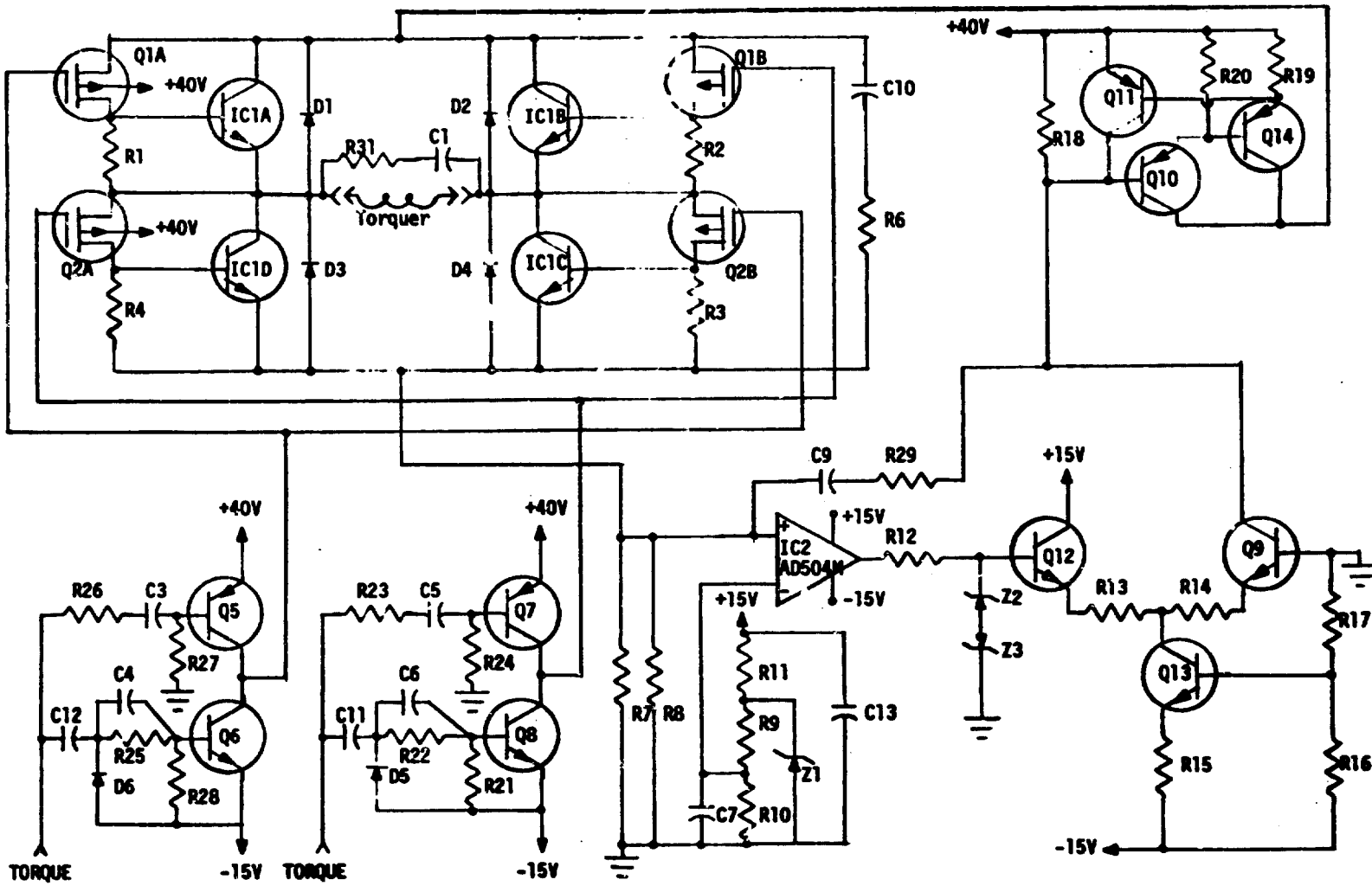

Figure 6. Torque Current Generator

torquer windings, respectively), thus the dc voltage drop across the torquer is (70.6 mA) (377) = 26.6V. Allowing 1V drop across each bridge transistor and 2.8V across the precision reference resistor (R7) leaves an 8V drop for the current-source transistor Q14. Originally, our design goal was 3°/sec full-scale torque, however, this required a 50V power supply and selection of transistors Q1, Q2, and IC1, since these units were rated at 40V, maximum. Also, we could not use the CMOS switch design of last period (1) due to the increase of the power-supply from +15V to +40V, thereby requiring a bridge-driver circuit utilizing dual-monolithic PMOS switches (Q1, Q2) similar to the earlier design of McKnight (3), and a new buffer circuit to interface the torque command signal from the +15V digital supply with the +40V TCG supply.

Other basic differences between the earlier TCG designs and the present Gyroflex TCG design are as follows:

1. Since the PMOS switches Q1 and Q2 are not as well matched as the CMOS switch (SCL4416) utilized previously, there were larger transient feed-through signals present at the input to the IC2 comparator. Unfortunately IC2 has a slow response with a slew-rate limitation less than 0.1V/μ-sec. Hence, we added a fast feed-forward path through R29 and C9 to the base of Q10, thereby lowering the transient feed-through error across R7 to a pulse less than 1V in amplitude and 0.5μ-sec wide.
2. The previous current source used was in an emitter-follower configuration (See Fig. 9, page 47, Ref. 1). Unfortunately, this type of design was very sensitive to power-supply noise coupling through directly to the H-Switch bridge. Inverting the current-source transistor Q14 considerably reduced this problem.

3. To eliminate spiking occurring at the transition of positive-to-negative torque switching, it was necessary to add the RC compensation network, R6 and C10.
4. Transistor Q11 was added for a short-circuit current limit of 250 mA to protect Q14.

For a complete description of the remaining parts of the TCG, the reader is referred to our detailed discussion, pages 46-51, Ref. 1.

Digital Control Electronics (DCE)

A complete description of the basic operation of the DCE is found in Ref. 1, pages 54-60. The schematic of the Gyroflex DCE is shown in Figure 7. This circuit differs from previous DCE designs as follows:

1. To eliminate the "race" or "glitch" problems encountered previously using the 4040 12-stage ripple counter, the current design uses the IC3 SCL4404, an 8-stage counter that is synchronously clocked. In order to obtain the correct scaling down to 2.4 kHz from the 1.2288 MHz crystal clock, it was necessary to add an additional divide-by-two stage, IC2A, to obtain 614.4 kHz The 614.4 kHz thus becomes the overall system clock, and its $\overline{Q}$ output $\overline{(614.4\ kHz)}$ is the data output clock.
2. The blanking signals (0-15 and 241-256) are obtained using one 4028 BCD-to-Decimal Decoder, instead of two as used previously. This change should have been made in our earlier designs.
3. Experiments at MSFC on earlier models of the DCE disclosed problems in obtaining correct scale factor counts when the blanking signals were used to re-set the J-K Flip Flop (IC5)

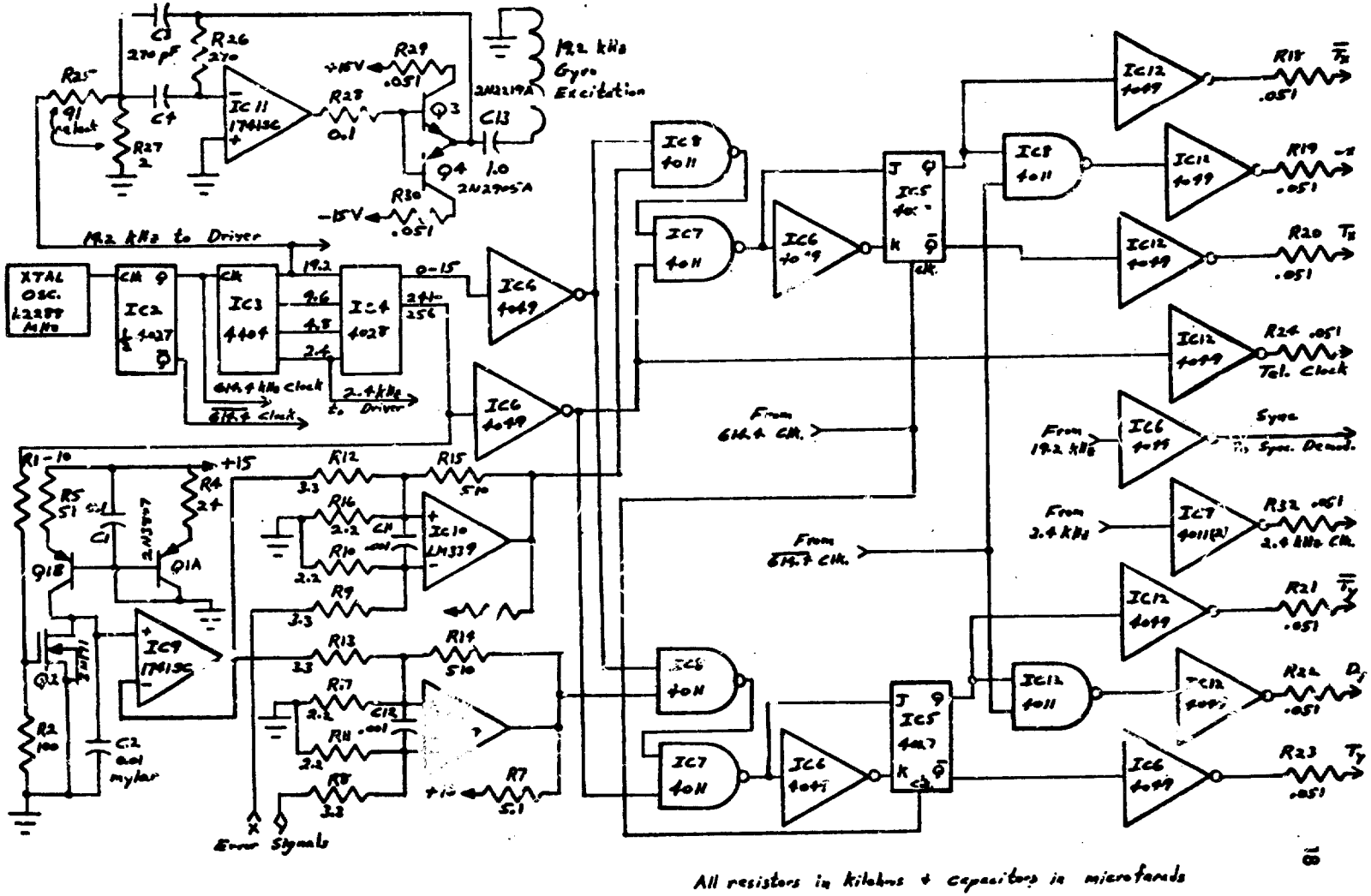

All resistors in kilohms & capacitors in microfarads

Figure 7. Digital Control Electronics

circuit. These problems were alieviated by a NAND operation of the blanking signals with the output signals of the comparators, before driving the IC5 Flip-Flops.

4. Because both the Q and $\overline{Q}$ outputs of IC5 are required to drive the TCG H-Switch, we decided to buffer these output torque command signals (shown as T and $\overline{T}$ in Figure 7), as well as the Data output signals (D_x and D_y).
5. The lowest count frequency (2.4 kHz) was brought out to use as a synchronized drive signal for the 1-sec or 10-sec reset signals to the external Data Counter circuits.
6. The signal generator circuit that converts the 19.2 kHz square-wave signal to a synchronous sinusoidal signal was increased in gain to furnish a 21.5V p.p signal to the primary of the gyro excitation transformer.

Spin-Motor Power Supply

A synchronized two-phase power supply of 480 Hz frequency is obtained by using the 19.2 kHz signal from the DCE, and dividing by two sections (using the 4018 divide-by-N counter) of 10 and 4 to obtain two 480 Hz output square waves, separated by 90 degrees. Each of these output signals is amplified through a separate power gain stage, the output of these stages driving the appropriate motor phase winding. The circuit schematic is shown in Figure 8, with IC1 and IC2 dividing by a total of 40, IC4 and Q5-Q8 being the power amplifier for the A phase output, with IC3 and Q1-Q4 being the B phase amplifier. The output drives are square-wave signals, 90 degrees apart, with $\pm$ 9.5V peak amplitudes. The total measured current drain

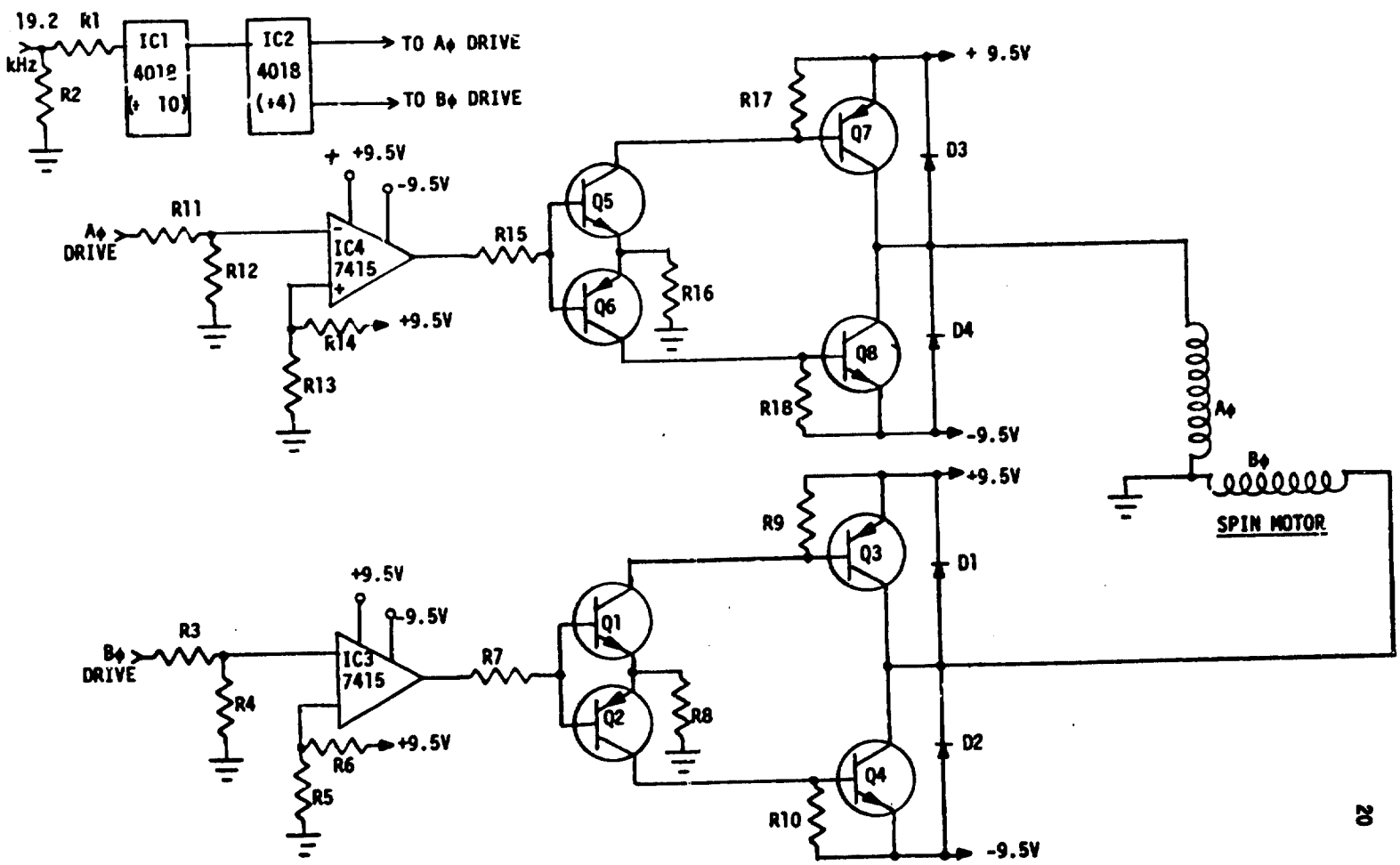

Figure 8. Gyroflex Spin-Motor Power Supply

from the power supplies was approximately 300 mA on start-up, and 140 mA normal running current.

DC-TO-DC Converter Power Supply

A schematic of the 28V input to ±15V, +40V and ±9.5V output dc-to-dc converter is shown in Figure 9. This converter was designed by Bill Baker of MSFC. The input dc voltage is converted to a regulated +33V, by the switching regulator circuit of Q1, Q2, Q5, L1, and CR2. The reference voltage is obtained by CR3-CR5, and the negative voltage reference of -3.2V at the emitter of Q2. The switching regulator design allows the input voltage to vary over a broad range of 24V to 32V, while still maintaining the output voltage of +33V constant to the push-pull switching primary transistors Q3-Q4. This regulation is accomplished by a duty-cycle variation of the switching regulator transistors Q1 and Q5 from 33% (at 24V input) to 10% (at 32V input).

Since the voltage applied to Q3 and Q4 is fixed, the output secondary voltages are therefore held constant. The push-pull transistors Q3-Q4 are alternately saturated (conducting) and open-circuited (non-conducting) at a operating frequency of 7 kHz, determined primarily by the saturable inductor L2, along with R4 and R5. Since the transformer T1 remains linear, its losses are low, and the overall efficiency of the converter is high.

The +15V output is obtained from a series-regulated circuit comprising Q6, Q7 and IC1. The -15V output is similarly connected. Initially the spin-motor voltage supply of ±9.5V was obtained by a simple full-wave rectifier circuit, however the output impedance of this supply was high, causing large ripple variations when connected to the two-phase spin motor circuit. We therefore added additional turns to the secondary windings and

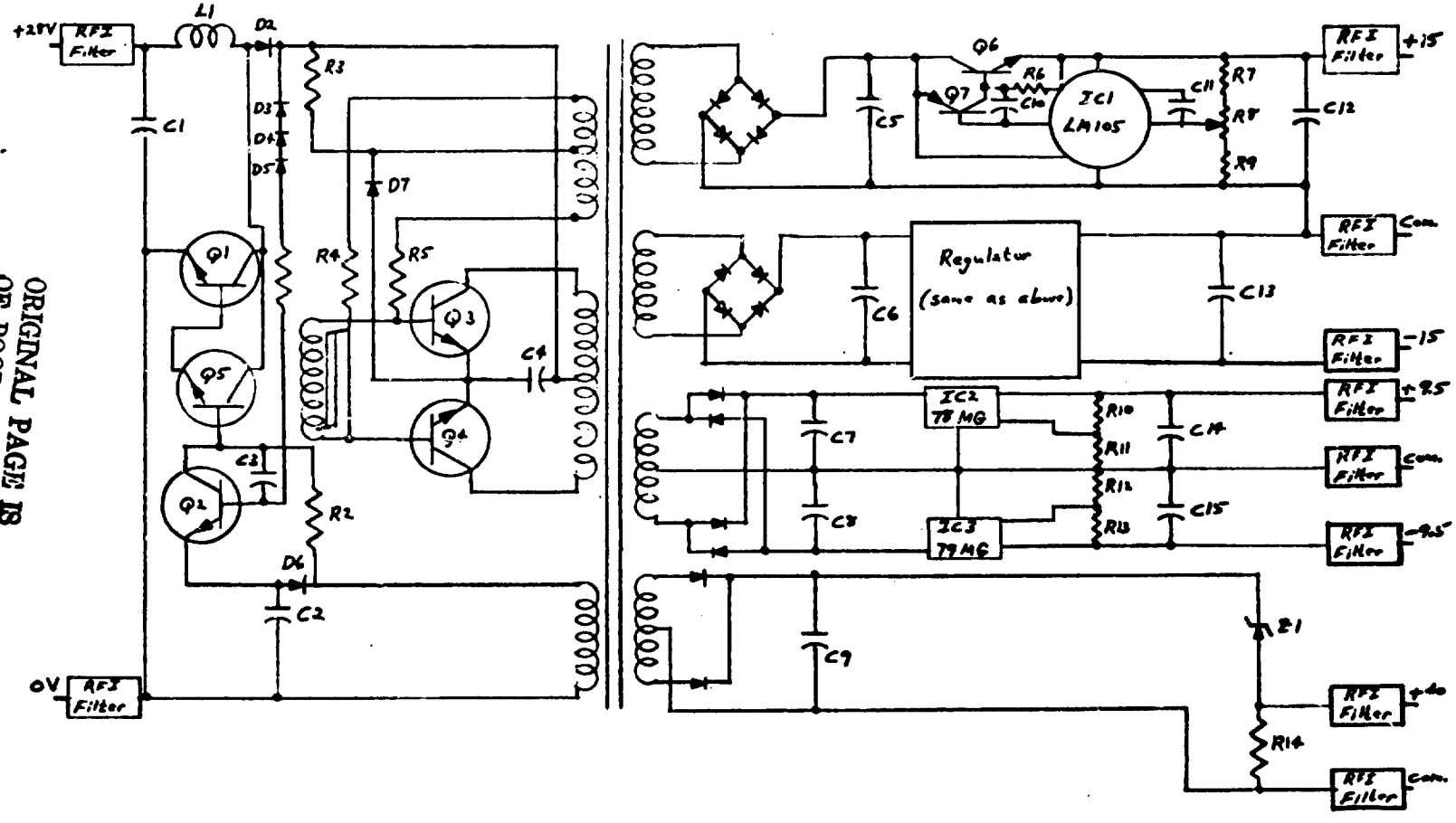

Figure 9. DC-to-DC Converter Power Supply

inserted the 78MG and 79MG 4-terminal series regulators to alleviate these problems. Even, then, it was necessary to add large de-coupling capacitors for the $\pm$ 9.5V outputs.

The +40V supply (used in the TCG H-Switch circuit) was initially designed for +50V output, since our original intention was to torque at 3 degrees/sec. Rather than re-winding the secondary winding for this supply for +40V output, we added a 10V Zener diode to drop the voltage.

With +28V input, and operating at fully-loaded outputs, the primary current was 0.68A, giving an overall efficiency of 58%. If the secondary turns on the +40V output supply were reduced from 77T to 61T, and Z1 removed, the efficiency should increase to 65%. A further increase in efficiency (to approximately 70%) could be obtained by reducing the series voltage drop across IC2 and IC3 by reducing the secondary turns from 25 to 22 on the $\pm$9.5V output supply.

CHAPTER IV

SYSTEM BREADBOARD EVALUATION

In this chapter, we present some observations and measurements obtained in the experimental evaluation of the breadboard version of the two-axis rebalance loop used with the Kearfott Gyroflex (S/N 4993). These results are primarily qualitative in nature since a detailed quantitative evaluation requires a precision rate table.

Transient Feedthrough

The switching of the torquer current, which is an innate characteristic of pulse rebalance systems, causes a transient feedthrough signal at the pickoff output (Figure 10) for the Kearfott Gyroflex used in our rebalance loop. It appears that these transients are due to energy transfer around the inertial element via both magnetic and electric fields. This phenomena can be accounted for by a signal transfer path that bypasses the inertial element. Of course, this is a very undesirable situation which can strongly influence the loop transmission and consequently affect such important loop characteristics as closed-loop bandwidth and oscillation stability.

The feedthrough signals at the beginning and the end of the interrogation period are always in the same time position relative to the 19.2 kHz pickoff signal (Figure 10). Thus, these signals appear as dc offsets at the output of the synchronous demodulator and could be compensated with a dc balance signal. There may be some problem, however, with dynamic range violations in the ac section of the ESP if the transients are too large.

The interior feedthrough signal, which occurs inside the interrogation period, is not fixed in time relative to the 19.2 kHz signal, but depends on

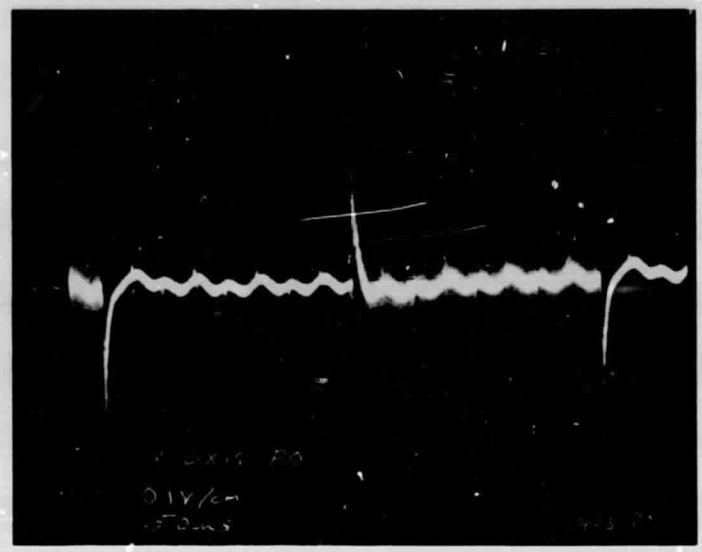

(a)

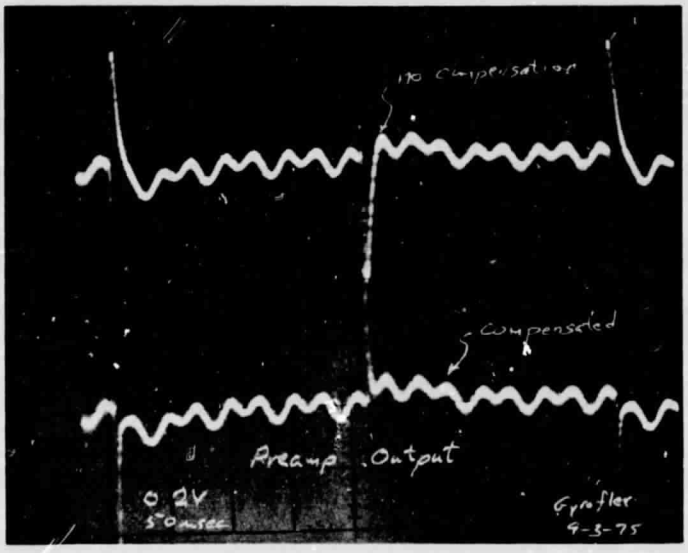

(b)

Figure 10. Photograph of the Transient Feedthrough Signals.

the torquing demand. As the position of this feedthrough signal moves over one complete cycle of the 19.2 kHz pickoff signal, the output of the synchronous demodulator caused by the feedthrough signal moves from some maximum negative dc level to some maximum positive dc level (or vice versa). So, the interior feedthrough signal inside the interrogation period may add to, subtract from, or have no effect on the legitimate error signal at the ESP output, all depending on the instantaneous torquing demand. This feedthrough signal cannot, therefore, be compensated with a simple dc balance signal. The interior feedthrough signal may cause a limit cycle oscillation of the duty cycle signal (Figure 3). The time amplitude of the duty cycle signal oscillation is usually no more than the period of the 19.2KHz pickoff signal.

We compensated for the transient feedthrough signals in our system by injecting the leading edge of the appropriate duty cycle generator signal through the high pass filter R_c, C_c of Fig. 5 into the ESP preamplifier at a summing node. In essence, we have added another signal path around the inertial element to cancel the undesired feedthrough signal. As shown in Fig. 10 b, the compensation, while adequate, is not perfect and other techniques should be investigated.

By simulating a rate input with current into the bias torquer, we have experimentally demonstrated that the transient feedthrough problem is very important and can strongly influence system bandwidth, phase margin and gain margin.

Rotor Induced Oscillations

It was expected (based on Gyroflex theory) that rotor induced oscillations (240Hz, 480Hz, etc.) would significantly contaminate the pickoff

signals and perhaps require the use of notch filters in the ESP. This was not the case in our system; the cluster of four poles (50Hz, 50Hz, 100Hz, 130Hz) in the ESP compensator was sufficient to bury the rotor induced oscillations in the random noise at the ESP output. These oscillations may be more significant for other Gyroflex units. In such cases, and if dynamic range constraints in the ac section of the ESP are not violated by the oscillations, we recommend the use of pole clusters to steeply roll off the loop transmission at frequencies below the lowest rotor oscillation frequency.

Loop Transmission Adjustments

The ESP midband gain was lowered from 63(36db) to 34.4(31db) to improve the measured gain margins for both X and Y loops. The resulting measured bandwidths and gain margins were

$$\text{X-axis} \quad \_\_ \quad f_{c\ell} = 3.7\text{Hz}, \qquad G_m \approx 12\text{db},$$

$$\text{Y-axis} \quad \_\_ \quad f_{c\ell} = 3.5\text{Hz}, \qquad G_m \approx 9.5\text{db}.$$

The measured gain margins above were worse-case values obtained by moving the interior feedthrough transient through one complete 19.2kHz period with the bias torquer. Even with the compensation for transient feedthrough, the gain margin did vary some over a complete cycle of the 19.2kHz pickoff signal indicating imperfect compensation. The loop gain was lowered by decreasing the resistor R7 in the ESP from 18k to 10k.

Interaction Between the X and Y Axes

Two kinds of interaction between the two axes were expected: (1) cross-modulation through the gyro dynamics, and (2) cross-modulation through the transient feedthrough phenomena. Our experiments indicated that the

total interaction between the axes had negligible effect on rebalance loop oscillation stability. There was, however, slight interaction between the axes as measured by counting data pulses from both axes when a rate was applied through the bias torquers. The averaged results for ten, 10 sec count intervals are listed below:

Axes interaction - Input to bias torquers

$$\Delta\overline{Y} = +16.5\% \qquad \Delta\overline{X} = -0.06\% \qquad \left(\frac{\Delta\overline{X}}{\Delta\overline{Y}} = \frac{1}{275}\right)$$

$$\Delta\overline{X} = +17.0\% \qquad \Delta\overline{Y} = -0.12\% \qquad \left(\frac{\Delta\overline{Y}}{\Delta\overline{X}} = \frac{1}{142}\right) \quad .$$

Although the interaction is too small to significantly affect loop stability, it can have a large influence on system accuracy. It is unknown how the interaction is proportioned between feedthrough and dynamic cross-modulation; measurements using a precision rate table must be performed to accurately determine the actual interaction.

Other Experimental Results

A photograph of the torque voltage pulse is shown in Fig. 11. The waveform for both axes shows excellent compensation of the torquer with a simple RC high-pass network connected across the torquer coil. The positive-going leading edge had a risetime of about 100 nsec while the negative-going edge had about a 30 nsec risetime. Note that these results are for approximately a 50 volt excursion in voltage across the torquer.

The data trains for both X and Y axes were photographed simultaneously and are shown in Figure 12. The data pulses are remarkably free of contaminating transients. The total pulse splatter observed on the oscilloscope appears to be much less than one-tenth of a data pulse.

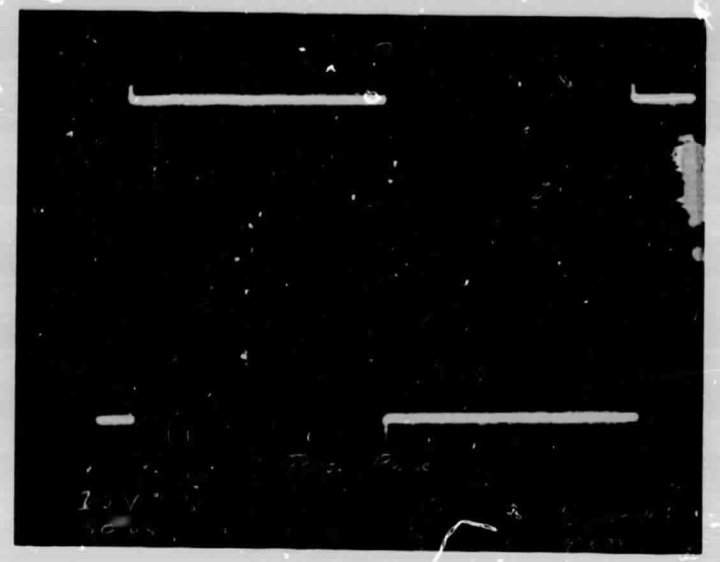

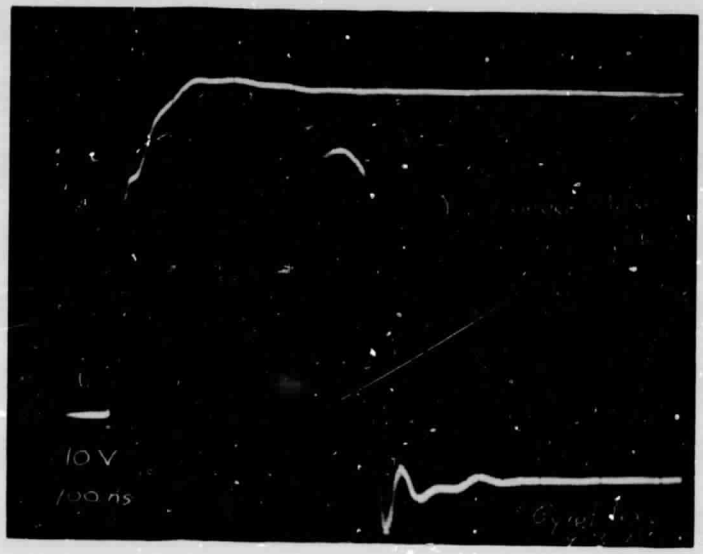

Figure 11. Torque Current Pulse.

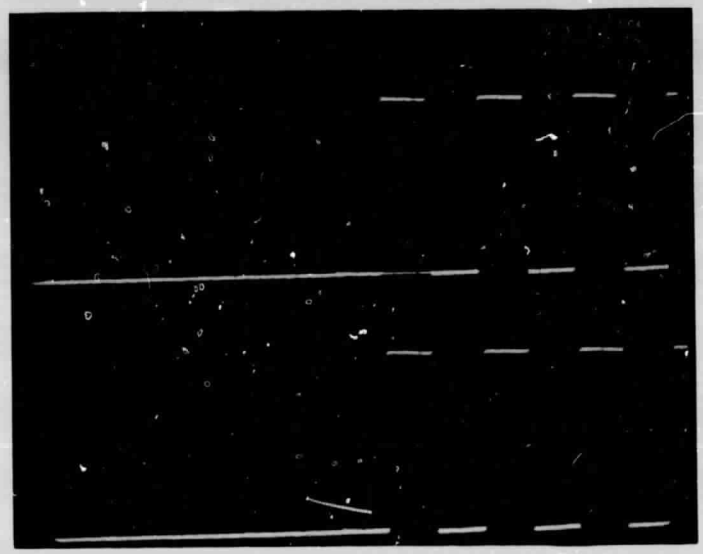

Figure 12. Data Trains.

Fig. 13 shows the system step function response for each axis with no input to the other axis. The input step is applied to the comparator input (DCE) through a 47K resistor. The response appears at the output of the ESP. For each axis there is negligible overshoot. The X-axis risetime is about 120 msec; the Y-axis risetime is about 80 msec which is somewhat faster.

When both axes are driven simultaneously with the same step signal, (Fig. 14a) there is no noticable change in the general structure of the responses relative to the single axis response with the other axis not driven. However, as shown in Fig. 14b, when one axis is driven, the other axis shows a small response which occurs at the transitions of the input step function. Further studies will be necessary to discover the cause of this interaction.

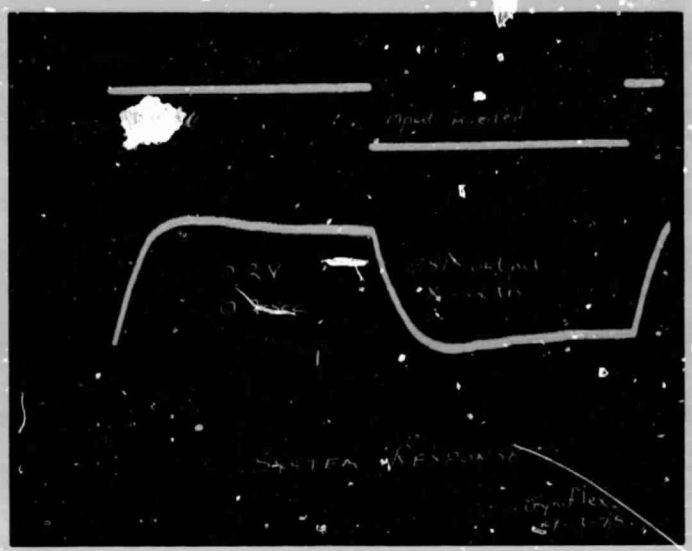

(a)

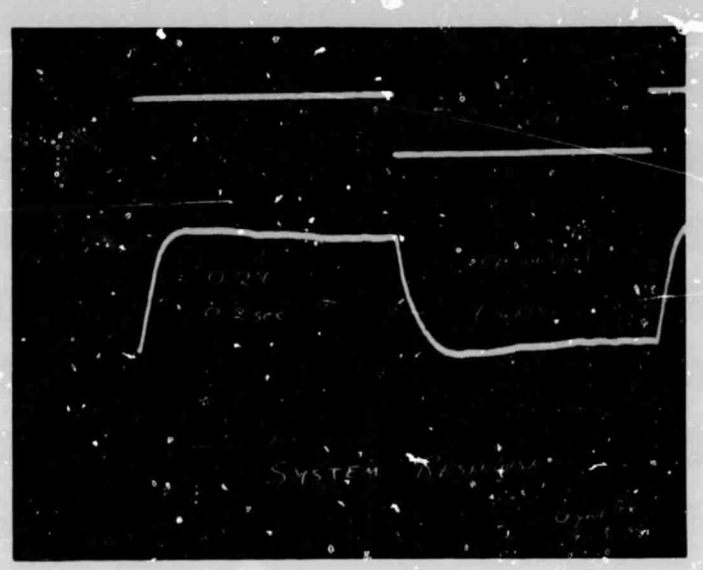

(b)

Figure 13. System Response-Each Axis.

(a)

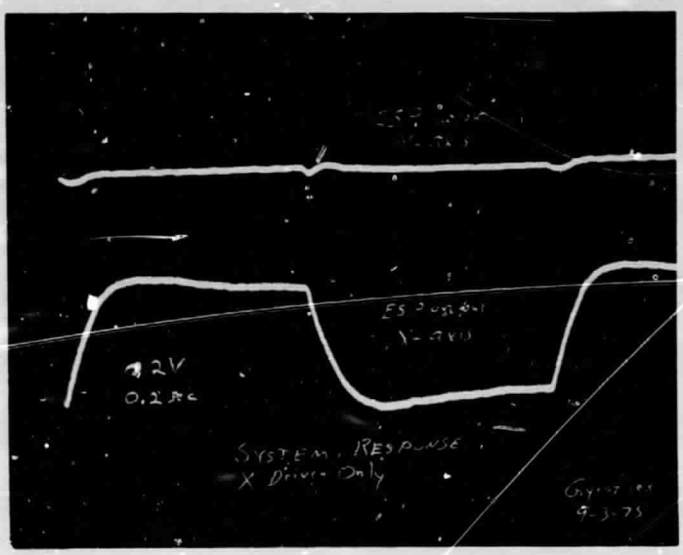

(b)

Figure 14. Interaction Effects in the System Response.

CHAPTER V

CONCLUSIONS AND RECOMMENDATIONS

Gyroflex Model

There seems to be confusion on the correct model for the Gyroflex. Much of the published theoretical work* predicts that the gyro pick-off output will have large amplitude rotor frequencies present and enough interaction between axes to require cross-coupling of the rebalance loops to have a stable system. Neither of these predictions were confirmed by our work with the Kearfott Gyroflex S/N 4993. Also the second gyro pole at f $\approx$ 0.031 Hz determined from the transfer function given for the S/N 4145 Gyroflex (2) did not exist in our unit. There seems to be a dearth of information on the measurement of the Gyroflex transfer function. We recommend that a program be launcned to experimentally characterize the Gyroflex in considerable detail.

Improved Gyro Torquer

The high voltages necessary to drive high currents through the gyro torquer place severe constraints on the design of the H-switch. The solution to this problem is the development of gyro torquers with much lower resistance.

Transient Feedthrough Problems

Methods should be developed for eliminating the transient feedthrough in the Gyroflex. One method would be to design special shielding into the

---

* See the excellent summary and extensive list of references on the theoretical work pertaining to dry tuned two-degree-of-freedom gyroscopes- Reference 4.

gyro stucture to block transient transmission. This may be difficult to implement and may compromise other structual requirements.

The cancellation techniques used with our first system reported here could perhaps be refined to more effectively subtract out the feedthrough signal, but, it will be difficult to generate a subtraction signal that will completely remove the feedthrough.

Perhaps the most promising method for solving the transient feedthrough problem is the complete removal of the feedthrough signal from the ESP signal with electronic gating techniques. Electronic gating technology is highly developed especially in such fields as nuclear instrumentation. Since we know when the feedthrough signal is going to occur, in principle, we should be able to remove it with a fast linear gate. We have several ideas for implementing such a gate but have not yet tested them in the laboratory.

REFERENCES

1. E. J. Kennedy, T. V. Blalock, W. L. Bryan, and K. Rush, "High-Resolution Width-Modulated Pulse Rebalance Electronics For Strapdown Gyroscopes and Accelerometers," Technical Report TR-EE/EL-2, for NASA under contract NAS8-27296/DCN 1-1-40-10230, Sept. 23, 1974.

2. R. F. Cimera, Trip Report, NASA-MSFC, "Test Evaluation of Gyroflex Gyro S/N 4145." Feb. 1, 1971.

3. R. D. McKnight, T. V. Blalock and E. J. Kennedy, "Design of a Torque Current Generator for Strapdown Gyroscopes," University of Tennessee, Electrical Engineering Technical Report TR-EE/EL-1, August 1974.

4. D. E. Coffman, "Feasibility Study of a Digital Rebalance Loop For a Dry Tuned TDF Gyro", Scientific Report S-28, University of Tennessee, Knoxville, May 31, 1974.